

#### ARTICLE



Check for updates



## Experimental $k_s$ estimation: A comparison of methods for Corynebacterium glutamicum from lab to microfluidic scale

Simone Schito<sup>5</sup> | Stephan Noack<sup>5</sup> | Jochen Büchs<sup>3</sup> | Alexander Grünberger<sup>1,2,6</sup>

#### Correspondence

Alexander Grünberger, Microsystems in Bioprocess Engineering, Institute of Process Engineering in Life Sciences, Karlsruhe Institute of Technology, 76131 Karlsruhe, Germany. Email: alexander.gruenberger@kit.edu

## Funding information

Deutsche Forschungsgemeinschaft: Bundesministerium für Bildung und Forschung

#### **Abstract**

Knowledge about the specific affinity of whole cells toward a substrate, commonly referred to as  $k_s$ , is a crucial parameter for characterizing growth within bioreactors. State-of-the-art methodologies measure either uptake or consumption rates at different initial substrate concentrations. Alternatively, cell dry weight or respiratory data like online oxygen and carbon dioxide transfer rates can be used to estimate  $k_s$ . In this work, a recently developed substrate-limited microfluidic single-cell cultivation (sl-MSCC) method is applied for the estimation of  $k_S$  values under defined environmental conditions. This method is benchmarked with two alternative microtiter plate methods, namely high-frequency biomass measurement (HFB) and substrate-limited respiratory activity monitoring (sI-RA). As a model system, the substrate affinity k<sub>5</sub> of Corynebacterium glutamicum ATCC 13032 regarding glucose was investigated assuming a Monod-type growth response. A k<sub>S</sub> of <70.7 mg/L (with 95% probability) with HFB,  $8.55 \pm 1.38$  mg/L with sl-RA, and  $2.66 \pm 0.99$  mg/L with sl-MSCC was obtained. Whereas HFB and sl-RA are suitable for a fast initial  $k_S$ estimation, sl-MSCC allows an affinity estimation by determining  $t_D$  at concentrations less or equal to the  $k_S$  value. Thus, sl-MSCC lays the foundation for strainspecific k<sub>S</sub> estimations under defined environmental conditions with additional insights into cell-to-cell heterogeneity.

#### **KEYWORDS**

affinity constant, cell-to-cell heterogeneity, Corynebacterium glutamicum, microfluidic single-cell cultivation, Monod growth kinetics, respiratory activity monitoring

#### 1 | INTRODUCTION

The growth rate  $\mu$  is one central parameter for the characterization, comparison, and classification of cellular processes. To predict microbial growth behavior, Monod (1949) established the first

growth kinetic model in 1949 while considering the bioavailability of the substrate (Equation 1). Within this empirical relationship,  $k_s$ denotes the affinity of a bacterium toward a corresponding substrate S with the concentration  $c_s$  and marks the concentration, where half of the specific maximum growth rate  $\mu_{max}$  is reached (Ferenci, 1999).

Heiko Steinhoff and Maurice Finger contributed equally and share first authorship.

This is an open access article under the terms of the Creative Commons Attribution-NonCommercial License, which permits use, distribution and reproduction in any medium, provided the original work is properly cited and is not used for commercial purposes. © 2023 The Authors. Biotechnology and Bioengineering published by Wiley Periodicals LLC.

1288

<sup>&</sup>lt;sup>1</sup>Multiscale Bioengineering, Bielefeld University, Bielefeld, Germany

<sup>&</sup>lt;sup>2</sup>Center for Biotechnology (CeBiTec), Bielefeld, Germany

<sup>&</sup>lt;sup>3</sup>AVT - Biochemical Engineering, RWTH Aachen University, Aachen, Germany

<sup>&</sup>lt;sup>4</sup>Institute of Biotechnology, RWTH Aachen University, Aachen, Germany

<sup>&</sup>lt;sup>5</sup>Institute of Bio- and Geoscience, IBG-1: Biotechnology, Jülich, Germany

<sup>&</sup>lt;sup>6</sup>Microsystems in Bioprocess Engineering, Institute of Process Engineering in Life Sciences, Karlsruhe Institute of Technology, Karlsruhe, Germany

The growth of cells in bioprocesses is affected by biological, chemical, and physical factors (Takors, 2012). In large-scale bioreactors, gradients of the substrate, dissolved gases, and pH occur through limiting capacities of engines, resulting in reduced input of power per volume, increased mixing times, and reduced k<sub>L</sub>a values (Bylund et al., 1998; Enfors et al., 2001; Junker, 2004; Mandenius, 2016). Hence, if the consumption rates of components required by the cells are higher than their supply, limiting conditions are present. This can lead to stress responses, which have a substantial impact on the yield and quality of the target product (Enfors et al., 2001). Therefore, access to precise  $k_s$  values is urgently required to model complex substrate gradients occurring within bioreactors by computational fluid dynamics. Additionally,  $k_S$  values are necessary to adjust the steady-state concentration of a carbon source, especially in bioprocesses operated in chemostat mode, to secure an efficient conversion of substrate into biomass (Harrison, 1973).

State-of-the-art estimation of  $k_{\rm S}$  is based on measuring specific substrate uptake rates  $q_{\rm S}$  within the exponential growth phase (Kell & Sonnleitner, 1995). Uptake rates  $q_{\rm S}$  are determined as a function of substrate concentration  $c_{\rm S}$  and correspond to the ratio of growth rate  $\mu$  to the biomass yield  $Y_{\rm X/S}$  in accordance with Equation (2). This lays the foundation to estimate  $k_{\rm S}$  by incorporating the Monod expression (Equation 1) and rearranging for  $k_{\rm S}$  (Equation 3) (Schmideder et al., 2015). The approach can be extended for chemostat cultivations under the condition that no residual concentration is present in the effluent by replacing the substrate concentration  $c_{\rm S}$  with the feed concentration  $c_{\rm S,feech}$  as well as the growth rate with the set dilution rate D (Equation 4) (Graf et al., 2020).

$$q_{\rm S} = \frac{\mu}{Y_{\rm X/S}},\tag{2}$$

$$k_{\rm S} = c_{\rm S} \cdot \left( \frac{\mu_{\rm max}}{q_{\rm S} \cdot Y_{\rm X/S}} - 1 \right), \tag{3}$$

$$k_{\rm S} = c_{\rm S,feed} \cdot \left(\frac{\mu_{\rm max}}{D} - 1\right). \tag{4}$$

Mainly three methods are reported in the literature to determine uptake rates  $q_{\rm S}$ , including high-performance liquid chromatography (HPLC) (Senn et al., 1994), enzymatic assays (Graf et al., 2020), or liquid scintillation counting (Lindner et al., 2011). However, liquid scintillation counting is only applicable if a labeled substrate such as  $^{14}$ C glucose is used. Alternative approaches to estimate the  $k_{\rm S}$  value are to measure the oxygen uptake rate (OUR) or the oxygen transfer rate (OTR) of aerobic growing cells, which correlates to growth (Stöckmann et al., 2003; Wechselberger et al., 2013). With the biomass concentration  $c_{\rm X}$  and the biomass yield on oxygen  $Y_{\rm X/O2}$ , the  $k_{\rm S}$  can be estimated according to the following equation:

$$k_{\rm S} = c_{\rm S} \cdot \left( \frac{\mu_{\rm max} \cdot c_{\rm X}}{OUR \cdot Y_{\rm X/O_2}} - 1 \right). \tag{5}$$

Respirometry methods for the estimation of kinetic parameters have been used more frequently and can deliver similarly precise  $k_{\rm S}$  estimations in comparison to established chemostat methods (Legan & Owens, 1987; Oliveira et al., 2009). These methods often rely on experiments in a respirometer but can also be conducted in situ through pulse respirometry (Goudar & Strevett, 1998; Ordaz et al., 2008).

Reported  $k_S$  values are scarce even for prominently used organisms. Corynebacterium glutamicum is recognized as a model organism in bioprocess engineering and industrial microbiology for its broad capabilities as a producer of value-added goods like amino acids (Hermann, 2003), organic acids (Wendisch et al., 2006), polymer precursors (Becker et al., 2018), aromatic chemicals (Wendisch et al., 2016), and proteins (Freudl, 2017). Moreover, C. glutamicum stands out for its robustness in large-scale applications (Graf et al., 2020; Vertès et al., 2012). However, even for this industrialrelevant organism, only a few published  $k_S$  values are available regarding glucose (Graf et al., 2020; Lindner et al., 2011; Uhde et al., 2013). As stated by Kovárová-Kovar and Egli, this is due to the fact, of analytical difficulty in monitoring substrates at growthcontrolling concentrations (Kovárová-Kovar & Egli, 1998). The applied state-of-the-art methods for a high precision  $k_S$  estimation are technically very complex, and even though they primarily provide merely extrapolated values, if liquid scintillation counting was not used.

This study demonstrates a microfluidic method and compares this method to two microtiter plate methods for estimating  $k_S$  values using C. glutamicum ATCC 13032 as a model organism to expand the biochemical engineering toolbox. For all methods, a Monod-type response of the specific growth rate is assumed to estimate  $k_{\rm S}$ . The first microtiter plate method is based on a computational approach for uncertainty quantification and relies on high-frequency biomass observations (HFB). This is accomplished with an end-to-end Bayesian modeling approach, according to Helleckes et al. (2022). The second method utilizes the newly developed micro(µ)-scale Transfer rate Online Measurement (µTOM) (Dinger et al., 2022) device for high-throughput respiratory activity measurements. Substrate-limited respiratory activity (sl-RA) monitoring determines the change in the OTR after spiking a defined glucose concentration, which correlates for aerobic growing cells with the growth rate. These microtiter plate methods are compared with the substrate-limited microfluidic single-cell cultivation (sl-MSCC) method. Novel microfluidic single-cell cultivations (MSCC) allow the cultivation of cells in defined environments (Wang et al., 2010), which can be maintained even for substrate-limiting conditions (Lindemann et al., 2019). This technology was applied to estimate the  $k_S$  value of C. glutamicum ATCC 13032 regarding protocatechuate acid (PCA) as a carbon source (Lindemann et al., 2019). Burmeister et al. (2021) used the same approach and estimated the lysine affinity for the lysine auxotrophic C. glutamicum ΔlysA pEKEx2-eYFP strain. However, MSCC as a technology has not yet been systematically established as a tool for k<sub>S</sub> estimation. It is unclear how comparable results are to conventionally established methods since studies on main carbon sources like glucose have not been performed to date. Finally, presented technologies (HFB,

Wiley Online Library on [17/08/2023]. See the Term

sl-RA, and sl-MSCC) are compared with literature values and future application fields of each individual method are pointed out.

#### 2 | MATERIALS AND METHODS

## 2.1 | Bacterial strain growth media

The bacterial strain *C. glutamicum* ATCC 13032 was used in this study. Cultivations were performed with modified CGXII medium (Unthan et al., 2014), containing per liter of distilled water 20 g (NH<sub>4</sub>)<sub>2</sub>SO<sub>4</sub>, 1 g K<sub>2</sub>HPO<sub>4</sub>, 1 g KH<sub>2</sub>PO<sub>4</sub>, 5 g urea, 13.25 mg CaCl<sub>2</sub>·2H<sub>2</sub>O, 0.25 g MgSO<sub>4</sub>·7H<sub>2</sub>O, 10 mg FeSO<sub>4</sub>·7H<sub>2</sub>O, 10 mg MnSO<sub>4</sub>·H<sub>2</sub>O, 0.02 mg NiCl<sub>2</sub>·6H<sub>2</sub>O, 0.313 mg CuSO<sub>4</sub>·5H<sub>2</sub>O, 1 mg ZnSO<sub>4</sub>·7H<sub>2</sub>O, 0.2 mg biotin, 37.5 mg citrate, 42 g MOPS, and 40 g p-glucose, unless stated otherwise. Similar to previous studies, PCA was replaced by citrate as iron chelator (Ho et al., 2022). Citrate as a potential available carbon source can only be metabolized by *C. glutamicum* if the saline concentration of NaCl is at least 1 g/L (Liebl et al., 1989; von der Osten et al., 1989).

## 2.2 | High-frequency biomass observations and Bayesian Monod modeling

Microtiter plate batch cultivation experiments were carried out in a 48-well FlowerPlate (m2p-labs GmbH) incubated in a BioLector Pro (m2p-labs GmbH) (Figure 1a). Culture well A01 was inoculated to an initial biomass concentration of 0.25 g/L from a glycerol stock. The cultivation parameters were set to 1400 rpm, 85% humidity, and 30 °C. The online signals for biomass (backscatter; gain 3), dissolved oxygen pO<sub>2</sub> and pH were measured with a cycle time set to 1 min (Figure 1b). Detailed information on reference gain and filterset can be found in the raw data file online (Osthege & Schito, 2022). The FlowerPlate was covered with a gas-permeable sealing foil (m2p-labs GmbH) to prevent contamination and allow uniform gas exchange. Medium preparation and inoculation were performed manually under a laminar flow hood.

Raw data was parsed with bletl version 1.1.0 (Osthege, Tenhaef, Helleckes, et al., 2022; Osthege, Tenhaef, Zyla, et al., 2022). Backscatter observations between 2 and 9.5 h were removed from

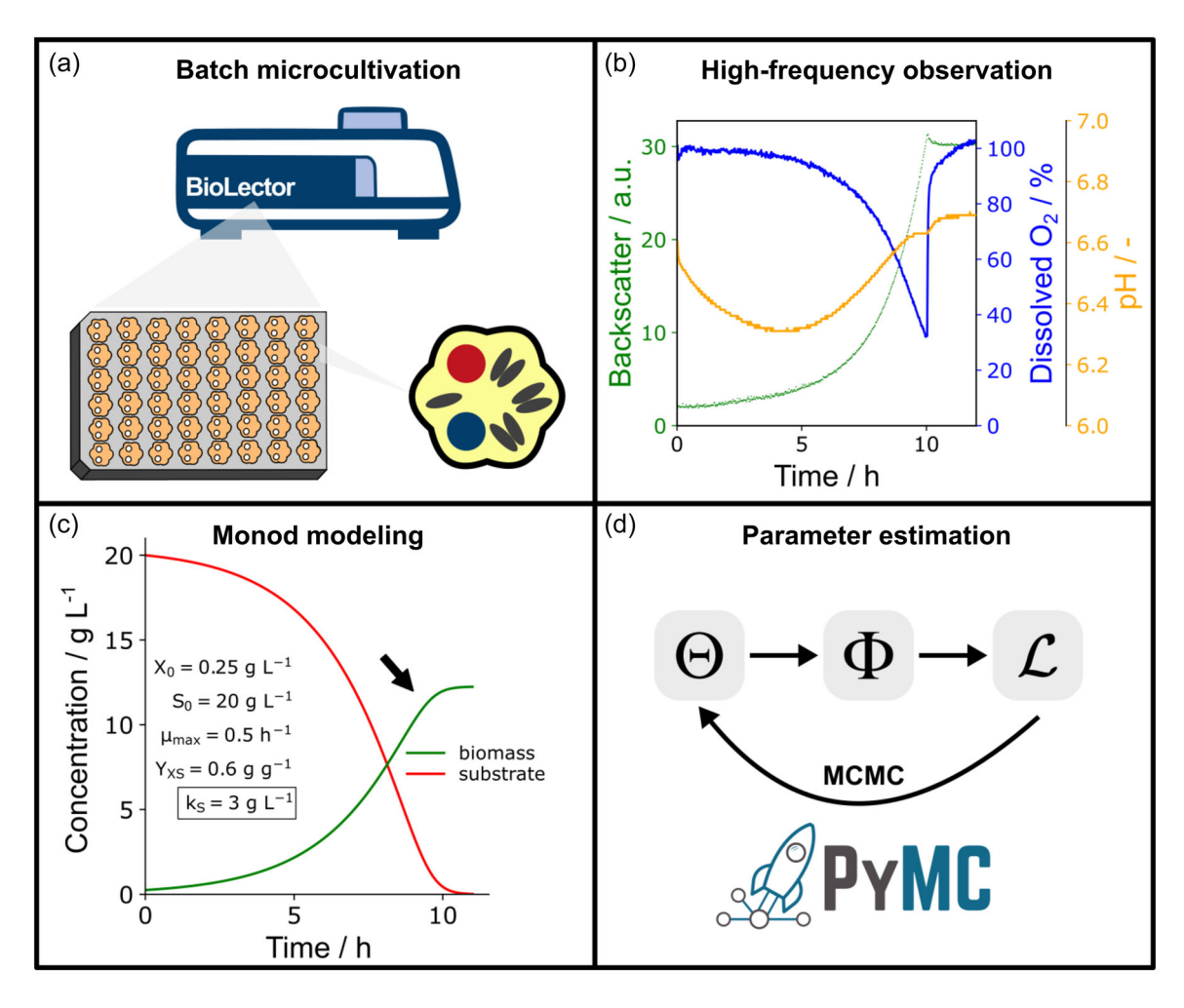


**FIGURE 1** Experimental setup and workflow for estimating the  $k_S$  of microbial cells with high-frequency biomass observations. (a) Microbioreactor batch cultivations with (b) high-frequency measurements of biomass-related backscatter. The  $k_S$  parameter in the (c) Monod model causes curvature (arrow) of the biomass trajectory. A computational model  $\Phi$  predicts the likelihood  $\mathcal{L}$  of observations. (d) Probabilistic parameter estimation obtained by Markov-chain Monte Carlo (MCMC) using the probabilistic programming library PyMC.

the data set to account for inaccuracies of the Monod assumption of approximately constant growth rate (Equation 1 with  $c_S\gg k_S$ ) for most of the exponential phase (Helleckes et al., 2022; Osthege, Tenhaef, Zyla, et al., 2022; Unthan et al., 2014). A biomass/backscatter calibration was established from reference backscatter measurements of a robotically prepared biomass dilution series of 48 biomass concentrations ranging from  $23.1\pm0.4\,\mathrm{g/L}$  to a 1000x dilution. The calibration model built with calibr8 version 6.5.2 (Osthege & Helleckes, 2022a) and the parameter estimates as well as a visualization of the fit, can be found in the supporting information

A Monod differential equation model was set up to describe the time series of biomass concentrations in the batch cultivation (Figure 1c). The respective equations and explanations are given in Chapter 3.1. The calibration model was used to relate predicted biomass concentrations with observed backscatter values, creating a likelihood for parameter estimation (Figure 1d). The model was implemented as a probabilistic model using Python packages PyMC version 4.0.0b6 (Wiecki et al., 2022) and murefi version 5.1.0 (Osthege & Helleckes, 2022b). Bayesian parameter estimation was performed by sampling the joint posterior probability distribution of model parameters using PyMC. In this iterative procedure, thousands of parameter sets are used to predict biomass trajectories with the ODE model and accepted or rejected based on the prior probability of the parameter values and how likely it would have been to observe the given data from such a trajectory. The result is a collection of thousands of parameter sets for the Monod model, each of which could plausibly explain the observed data. A detailed description of the method is given by Helleckes et al. (2022).

Here, the PyMC implementation of the DE-MCMC-Z algorithm (ter Braak & Vrugt, 2008) was used with 20,000 tuning and 50,000 draw iterations in four independent Markov chains. Convergence of the Markov-chain Monte Carlo (MCMC)-sampling was checked by validating that all  $\hat{R}$  < 1.01 using ArviZ version 0.12.0 (O. Martin et al., 2021). For detailed explanations of calibration modeling and the Bayesian modeling of batch cultivations using the Monod model, it can be referred to Helleckes et al. (2022). The full data set and code to reproduce the  $k_{\rm S}$  analysis using the high-resolution biomass and Bayesian ODE modeling approach are provided online (Osthege & Schito, 2022).

# 2.3 | Substrate-limited respiratory activity monitoring

For the respiratory determination of  $k_{\rm S}$ , deep-well microtiter plates Riplate RW (Ritter GmbH) with 96 wells were used. The OTR of every well was online monitored with the  $\mu$ TOM (Figure 2a) (Dinger et al., 2022). All wells were filled with 1 mL of inoculated culture. Cultivations were performed at a temperature of 30°C, a shaking speed of 800 rpm, and a shaking diameter of 3 mm. Precultures for inoculation were performed in 250 mL shake flasks with CGXII medium with 10 g/L glucose as the sole carbon source. The main culture was

inoculated with 5 (v/v)% from a stationary phase preculture and was also conducted in CGXII medium but with  $1\,g/L$  glucose.

After the initial batch cultivations, 100 µL glucose solutions with different concentrations were spiked into each well of the microtiter plate (Figure 2b). This resulted in a theoretical filling volume of 1.1 mL per well with final glucose concentrations of 0.0, 2.5, 5.0, 7.5, 10.0, 12.5, 15.0, 17.5, 20.0, 30.0, 40.0, 50.0, 60.0, 70.0, 80.0 100.0 mg/L. A multichannel multistepper pipette Eppendorf Research pro (Eppendorf) was used to spike all wells 2 min before the next OTR measurement phase started. The first 30 s of the measurement phase of the  $\mu TOM$  device were cutoff, and OTRs were determined by the oxygen partial pressure decrease within the next 2 min. The end of the initial batch and glucose depletion was indicated by a rapid decrease in the OTRs (Figure 2c), whereas the glucose spike resulted in a concentration-dependent fast increase of the OTR. The resulting OTRs after the spike with 0.0 mg/L of glucose were subtracted from all other resulting OTRs. A regression of these values to the Monod equation was performed with OriginPro (OriginPro 2020 9.7.0.188; OriginLab Corporation) to estimate the  $k_S$  value (Figure 2d).

## 2.4 | Substrate-limited microfluidic single-cell cultivation

## 2.4.1 | Design and microfluidic chip fabrication

The design of the microfluidic chip is based on a recently developed MSCC method from Lindemann et al. (2019). The MSCC systems consist of 12 arrays of "quasi" one-dimensional growth channels to restrict cell proliferation of a few cells (<15) along one axis (Figure 3a). These growth channels are open on both ends and connected to adjacent supply channels. There, the fresh medium flows with a high velocity to ensure a constant and defined medium supply to the growth channels. In total, one cultivation unit consists of 1440 growth channels.

A silicon wafer mold was fabricated with a two-layer photolithography process and served as a mold for PDMS (poly(dimethylsiloxane)) soft lithography (Grünberger et al., 2013). The construction and development of a siliconwafer was carried out according to the protocol of Täuber et al. (2020). During soft lithography, the siliconwafer was covered with PDMS in a ratio 10:1 between the base and curing agent (Sylgard 184 Silicone Elastomer, Dow Corning Corporation). Afterward, the wafer was degassed in a desiccator for 30 min and backed at 80 °C for 2 h (universal cupboard; Memmert GmbH). After this step, the PDMS chips were cut out from the wafer, cleaned three times with isopropanol, and blown dry with pressurized air. The cover glasses (D 263 T eco, 39.5 × 34.5 × 0.175 mm, Schott) for the microfluidic chip were also cleaned after the same protocol. Afterward, the PDMS chip and the cover glass were activated with O<sub>2</sub> plasma (Femto Plasma Cleaner; Diener Electronics) for 24 s with a power of 45% and assembled. Before the use, PDMS-glass bonding was strengthened by a 2 min bake at 80 °C.

0970290, 2023, 5, Downloaded from https:

com/doi/10.1002/bit.28345 by Forse

Wiley Online Library on [17/08/2023]. See the Term

for rules of use; OA articles are governed by the applicable Creative Common

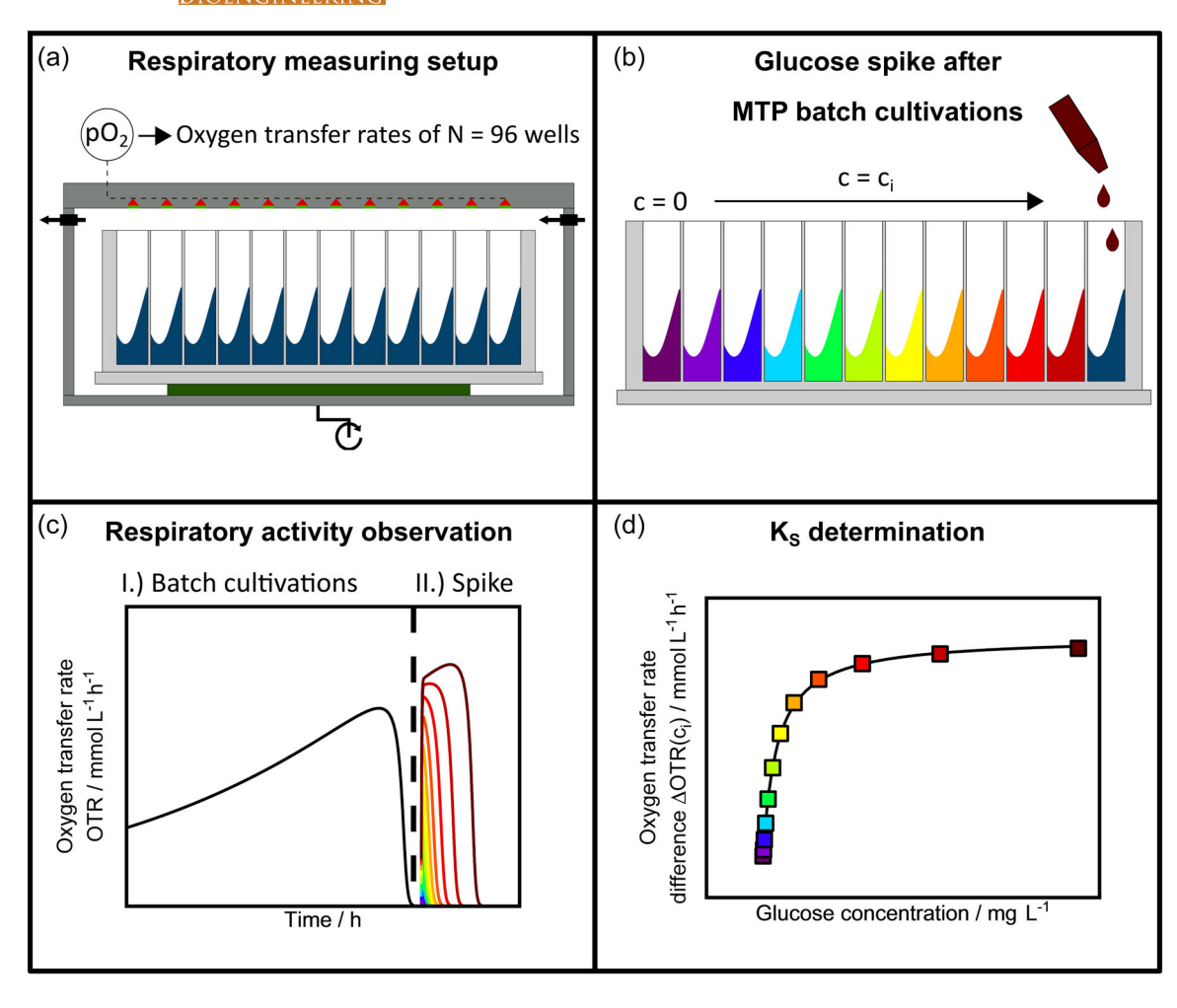


**FIGURE 2** Experimental setup and workflow for estimating the  $k_S$  of microbial cells with substrate-limited respiratory activity monitoring. (a) Micro( $\mu$ )-scale Transfer rate Online Measurement device ( $\mu$ TOM) for 96-deepwell microtiter plates. The figure for the  $\mu$ TOM device was adapted from Dinger et al. (2022). (b) Spike of varying substrate concentrations after the termination of the batch cultivations with 96 replicates. (c) Observation of the substrate-dependent oxygen transfer rates. (d)  $k_S$  determination based on Monod-type respiratory response.

## 2.4.2 | Single-cell cultivation

Overnight precultures of C. glutamicum were inoculated from glycerol stock in 10 mL CGXII medium in 100 mL flasks on a rotary shaker at 120 rpm. Cells from the overnight culture were transferred to inoculate a second shake flask culture with a starting OD<sub>600</sub> of 0.1 for harvesting of cells in the exponential growth phase. The cells were used to inoculate the microfluidic device manually through a syringe containing a cell suspension with an OD of approximately 0.6. Seeding of the growth channels was obtained by random trapping of cells. After successfully seeding, the microfluidic chip was connected to pressure-driven pumps (Flow EZ Pressure Controller; Fluigent) and controlled by software (All in One; Fluigent). An inlet pressure of 150 mbar was applied for a constant medium supply (Figure 3b) (Li et al., 2017). Afterward, growth kinetic studies in CGXII were performed containing concentrations from 0 up to 150 g/L glucose. The possibility of interactions between hydrophilic molecules such as glucose and PDMS as a hydrophobic polymer can be excluded (Toepke & Beebe, 2006). Each cultivation medium

was additionally sterile filtered to prevent channel clogging during microfluidic experiments.

## 2.4.3 | Live cell imaging, data analysis, and growth rate modeling

Time-lapse microscopy was performed using an inverted automated microscope from Nikon (Nikon Eclipse Ti2; Nikon). The microscope stage was surrounded with a cage incubator for optimal temperature control (Cage incubator; OKO Touch; Okolab S.R.L.). The microfluidic device was placed inside the cage incubator in an in-house fabricated chip holder. Additionally, the setup was equipped with a 100x oil objective (CFI P-Apo DM Lambda 100x Oil; Nikon GmbH), DS-Qi2 camera (Nikon camera DS-Qi2; Nikon GmbH), and an automated focus system (Nikon PFS; Nikon GmbH) to compensate the thermal drift during long term microscopy (Figure 3a). For each experiment, 80 positions containing several cultivation channels were selected manually and were managed with NIS-Elements Imaging Software

**FIGURE 3** Experimental setup and workflow for estimating the  $k_S$  of microbial cells with substrate-limited microfluidic single-cell cultivation (sl-MSCC). (a) Live cell imaging setup consisting of an inverted phase-contrast microscope and a microfluidic single-cell cultivation chip, allowing high-spatiotemporal resolution. (b) Single-cell cultivation performed under varying substrate concentrations. (c) Determination of  $t_D$  of the online-monitored time-lapse data. (d) Establishing a kinetic model based on a Monod-type response by the conversion of  $t_D$  into growth rates  $\mu$  to display growth as a function of glucose concentration to estimate  $k_{S,sl-MSCC}$ .

(Nikon NIS Elements AR software package; Nikon GmbH). Time-lapse images were recorded every 5 min.

Data analysis of the live-cell image sequences was performed using the open-source software Fiji 1.52 (Schindelin et al., 2012). For determining single-cell division events, one offspring cell was selected whose descendants were present until the end of the measurement. Based on the growth of this cell line, it can usually be guaranteed that at least 50 single-cell division events occurred. Two categories were differentiated for the case that a selected glucose concentration resulted in reduced growth. The first category describes cell growth for less than four generations, defined as no growth. The second category describes cases where less than 50 single-cell division events were observed. In this case, offspring of further descendants were considered for quantification to reach the minimum of at least 50 single-cell division events.

The doubling time of each offspring of the selected cell lineage was determined after the first division event through selection of the cell by using the integrated multipoint function of Fiji (Figure 3c).

This ensured a frame-independent tracking of temporally asymmetric divisions of daughter cells depending on the generation time. The respective mean values for  $t_D$  and growth rates were determined using the geometric mean (Phoenix, 1997). Here, extreme outliers with  $t_D > 1000$  min or  $t_D < 30$  min were not considered, because the formula for the determination of the standard deviation uses summation of squared errors. Therefore, the impact of extreme outliers is espically high for low sample sizes. We observed that doubling times of 1000 min or below 30 min generate a standard deviation equal to the mean. To avoid this, we neglected these extreme rare outliers when considiering our kinetics due to the loq frequency to determine an affinity reflecting more than 95% of the population. The first step in determining  $k_S$  is calculating the growth rate with each determined doubling time. The equation and explanation are stated in Chapter 3.1. Then, the corresponding geometric mean, including the standard deviation, is plotted as a function of the respective glucose concentration. A Monod kinetic fit is then established using OriginPro (OriginPro 2020 9.7.0.188;

0970290, 2023, 5, Downloaded from https

for rules of use; OA articles are governed by the applicable Creative Comn

OriginLab Corporation) (Figure 3d). The regression slope obtained from the logarithmic plot corresponds to  $k_s$ .

#### 3 | RESULTS AND DISCUSSION

### 3.1 | Comparison of methodologies

In this work, three unique methods for  $k_{\rm S}$  estimation are presented: HFB, sl-RA, and sl-MSCC. All methods assume a Monod-type growth response (Equation 1). Thereby, the  $k_{\rm S}$  value is always estimated by observing the growth under substrate limiting conditions. For the understanding of the different methodologies and their potentials as well as limits, a comparison is given regarding (1) cultivation workflows, (2) computational approaches for  $k_{\rm S}$  estimation, and (3) analytical procedures.

#### 3.1.1 | Cultivation workflows

HFB and sI-RA are based on microtiter cultivation systems (Figures 1 and 2). In contrast, sI-MSCC is based on MSCC devices (Figure 3). In the HFB workflow, the biomass is observed during a batch cultivation over time. The glucose is steadily consumed by the cells until complete glucose consumption, which is indicated by a sharp rise in the DO (Figure 1b). The rise in DO can be attributed to the fact that the glucose uptake rate is linked via growth to the OUR. The link of growth and OUR is utilized for  $k_s$  estimation with sl-RA. For the sl-RA, depletion of glucose after an initial batch cultivation is indicated by a drop in OTR (Figure 2c). In comparison to the HFB workflow, after the termination of the batch cultivation, different glucose solutions are spiked into the microtiter plate wells to adjust defined substrate levels. For the third alternative, sl-MSCC, defined and contrasting to the other methods, constant conditions are reached by perfusion with a medium containing a defined glucose concentration. Thereof, HFB and sl-RA are faster and easier to perform. Nonetheless, sl-MSCC provides a more defined environment due to perfusion and thereby, constant substrate concentrations even at limiting conditions. In contrast to sI-MSCC and sI-RA, where glucose concentrations are set by perfusion or spiking, the glucose concentration is only measured once at the onset of the stationary phase with a hexokinase assay for the HFB.

### 3.1.2 | Computational approaches for $k_s$ estimation

In HFB, a batch cultivation is monitored by backscatter measurements. For parameter inference, the parameter sets proposed by the MCMC algorithm are used to simulate biomass concentration trajectories using the differential model (Equation 6) based on the Monod equation (Equations 1 and 2). These concentration values are fed into an asymmetric logistic calibration model to predict the distribution of backscatter observations. This enables the model to

relate model parameters with observations, learning about how well a chosen parameter set describes the data. For a detailed explanation of this modeling procedure, see Helleckes & Osthege et al. (2022).

$$\frac{dc_X}{dt} = \mu_{\text{max}} \cdot c_X \cdot \frac{c_S}{k_S + c_S},$$

$$\frac{dc_S}{dt} = \frac{-1}{Y_{X/S}} \cdot \frac{dc_X}{dt}.$$
(6)

Instead of the biomass concentration  $c_X$ , the OTR is observed in sI-RA. The change in dissolved oxygen  $dO_L/dt$  is assumed to be negligible compared with the OUR, similar to Mühlmann et al. (2018) and Ihling et al. (2021). Hence, the OTR is used equivalently to the OUR (Equation 7). Data by Graf et al. (2020) indicate a linear correlation of growth rates (0.2–0.4 h $^{-1}$ ) and OURs and therefore, a constant  $Y_{X/O2}$ . However, this assumption is not necessarily true at very low growth rates. Only due to this simplified linearity assumption of the growth rate and the OTR, the sI-RA model is interchangeable with the models of the other methods. Thereby, the  $k_{\rm S}$  value can be estimated directly with the glucose concentration-dependent OTR and using a regression of the Monod equation.

s. t. OUR 
$$\gg \frac{dO_L}{dt}$$
, (7)

$$\mu = \frac{OTR \cdot Y_{X/O_2}}{c_X}.$$
 (8)

For sl-MSCC, single-cell doubling times  $t_D$  are determined. Under the assumption that both cells have the same size after splitting, the growth rate  $\mu$  can be calculated (Equation 9). Similar to sl-RA, a mathematical fit under the assumption of Monod-type response of growth is used to estimate the  $k_S$  value based on the glucose concentration-dependent growth rates.

$$\mu = \frac{\ln 2}{t_D}.\tag{9}$$

#### 3.1.3 | Analytical procedures

As a Mond-type growth response is assumed for all methods, the following analytical procedures are chosen to measure parameters correlating to the growth of *C. glutamicum*. For HFB, backscatter measurements are performed in a BioLector. In contrast, sl-MSCC allows single-cell tracking by inverted phase contrast microscopy. The sl-RA depends on the indirect growth tracking by monitoring the OTR. To this end, high-throughput OTR measurements are conducted in a  $\mu TOM$  device. The equipment for the presented methods is not available in every laboratory. However, the proposed approaches can be adapted for other devices and provide insight into the theoretical backgrounds behind  $k_S$  estimation.

## Substrate affinity $k_S$ estimations

The HFB method for  $k_S$  estimation takes the data from the microbioreactor batch cultivation, comprised of 464 backscatter observations after preprocessing and one simulated glucose measurement. Parametrization of the probabilistic Monod model was obtained with uninformative prior beliefs of the model parameters:  $S_0 \sim LogNormal(\mu = log(20\frac{g}{L}), \sigma = 0.1)$ ,  $X_0 \sim LogNormal$  $(\mu = \log(0.25\frac{g}{l}), \sigma = 0.1), \quad \mu_{\text{max}} \sim \text{Beta}(\mu = 0.4, \sigma = 0.1), \quad Y_{X/S} \sim \text{Beta}$  $(\mu = 0.6, \sigma = 0.05), k_S \sim Uniform(0, \infty)$ . Note that the prior information for  $k_{\rm S}$  constrains it to positive numbers but does not bias the model beyond that.

The MCMC sampling of the joint posterior probability distribution (Figure 4b) for these five parameters given the 119+1 observations and corresponding calibration models yielded a total of 200,000 parameter vectors, each corresponding to one possible trajectory of Monod kinetics. In Figure 4c,d, individual examples of such trajectories are drawn alongside a density band representing the posterior probability distribution of trajectories. Vertical violin plots show the 90% highest-density intervals of the posterior probability distributions of biomass (green) and substrate (blue) concentrations obtained from single measurements with the calibration model. These are the narrowest intervals containing the inferred parameter (here: biomass concentration) with a probability of 90%. Note that inferences from single backscatter observations resulted in much

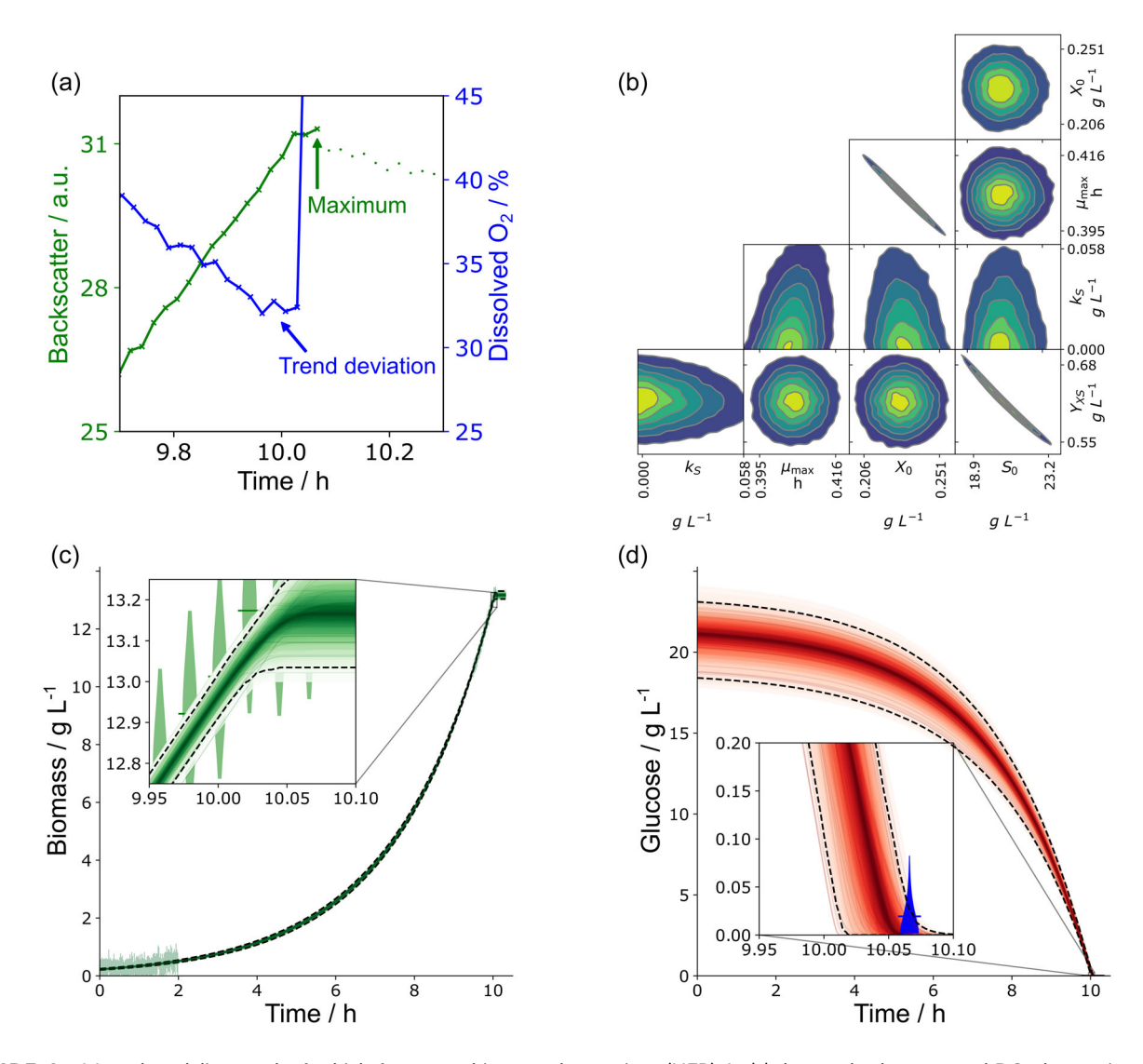


FIGURE 4 Monod modeling results for high-frequency biomass observations (HFB). In (a) the raw backscatter and DO observations of the transition from exponential to stationary phase show a deviation from the declining DO trend for three cycles (approx. 3 min) before a sharp rise in DO. (b) Data up to the first cycle after the rise was considered to infer posterior probabilities of the Monod model parameters. The  $Y_{X/S}$  and  $S_0$ as well as  $\mu_{max}$  and  $X_0$  parameters are strongly correlated. The highest probability density for the  $k_S$  parameter is near 0 mg/L. (c and d) Show the resulting distribution of biomass and substrate trajectories predicted from sampled parameter sets. Violins indicate the probabilities inferred from individual data points without the use of the Monod model. Thin lines indicate trajectories resulting from exemplary parameter sets. The dashed line indicates the highest density interval, around 90% of the probability mass.

larger uncertainty about biomass concentration than those obtained from ODE model trajectories (green bands, dashed lines). This is because ODE trajectories are constrained by the relatively rigid assumption of Monod-like growth and the combined information from 119 observations. Nevertheless, the curvature of trajectories is visible at timescales of approximately less than 1 min (Figure 4c,d). This asymmetric observation of "less than" corresponds to the marginal posterior distribution of  $k_{\rm S}$  exhibiting no lower tail toward 0 g/L, but a clear tail toward higher concentrations. In this case, 95% of the  $k_{\rm S}$  posterior probability distribution is <70.7 mg/L, corresponding to the interpretation that  $k_{\rm S}$  < 70.7 mg/L with a 95% probability according to this analysis. Since the 95% probability threshold is arbitrary, equally valid statements with slightly different interpretations can be provided:  $k_{\rm S}$  < 21.5 mg/L with a 50% chance (the median) or  $k_{\rm S}$  < 10.0 mg/L with a 26.4% chance.

In Figure 4b, two-dimensional marginals of the five-dimensional joint probability distribution are shown as kernel density estimates. These visualizations show that with this data set,  $k_{\rm S}$  is not correlated to other parameters of the Monod model, whereas  $\mu_{\rm max}$  is strongly correlated with  $X_{\rm O}$ , and  $Y_{\rm X/S}$  is strongly correlated with  $S_{\rm O}$ . These correlations are structural and well expected (Helleckes et al., 2022). If a lower  $S_{\rm O}$  is estimated,  $Y_{\rm XS}$  has to be higher to fit the biomass observations. Due to the strong Monod assumptions and the 464 backscatter observations, our posterior estimate for the  $\mu_{\rm max}$  of this batch is rather narrow with 90% of the probability mass in the interval [0.395, 0.416]  $h^{-1}$ .

For respiratory estimation of the  $k_{\rm S}$  with the sl-RA, 96 batch cultivations were performed simultaneously in a 96-deepwell plate. The online monitored OTR of these cultivations show an increase and, therefore, the initial growth of *C. glutamicum* for the first 3 h (Figure 5a). The rapid decrease of the OTR afterwards points to the depletion of the main carbon source glucose, which was only supplied with 1 g/L. The utilization of alternative carbon sources leads to a low

OTR of around 1 mmol/L/h, which is also progressively decreasing after 3.5 h (Figure 5a). As soon as glucose is spiked into the wells, growth, according to Monod (Equation 1), sets in. Only for the glucose spike concentration of 0 mg/L a lower OTR after spiking was measured with  $0.9 \pm 0.1$  mmol/L/h. The glucose-dependent OTRs are also depicted in Supporting Information: \$14-16. The differences between the OTR reference value at 0 mg/L and all other OTRs were calculated (Figure 5b). For spiked glucose concentrations of at least  $20\,\text{mg/L}$ , a constant  $\Delta OTR$  of  $2\,\text{mmol/L/h}$  is noticeable. The decreased  $\Delta$ OTR value for the condition with a glucose concentration of 100 mg/L could be subject to measurement variance or caused by a physiological explanation due to overflow metabolism. However, as this work focuses on the  $k_S$  value, this trend was not further investigated here. For glucose concentrations of 20 to 0 mg/L, the  $\Delta$ OTR is decreasing. With the regression to the Monod equation, a  $k_{\rm S}$ of 8.55 ± 1.38 mg/L was obtained with a coefficient of determination of  $R^2$  = 0.95. A logarithmic plot of Figure 5b is given in Supporting Information: \$17.

Growth experiments in CGXII with varying glucose concentrations were performed with *C. glutamicum* at 30 °C using sl-MSCC for 72 h. For the assurance that the distribution of the doubling time follows a Gaussian distribution, distributions of selected concentrations are shown as examples. At glucose concentrations of  $500\,\mathrm{mg/L}$  (Figure 6a), the average doubling time is about  $75\pm15\,\mathrm{min}$  with low variance. Furthermore, the single-cell  $t_D$  are normal distributed with a coefficient of determination of  $R^2=0.97$ . At glucose limiting concentrations, the dispersion and variance increase drastically, leading to  $t_D$  at  $5\,\mathrm{mg/L}$  of  $188\pm204\,\mathrm{min}$  (Figure 6b) and at  $2.5\,\mathrm{mg/L}$  of  $122\pm69\,\mathrm{min}$  (Figure 6c) with a coefficient of determination of  $R^2=0.76$  and  $R^2=0.89$ , respectively. We exclude technical bias at the concentration of  $5\,\mathrm{mg/L}$  due to limitations or gradients in nutrition. Thus, we are convinced that the nongaussian distribution is due to the limiting carbon-conditions itself. We speculate that the

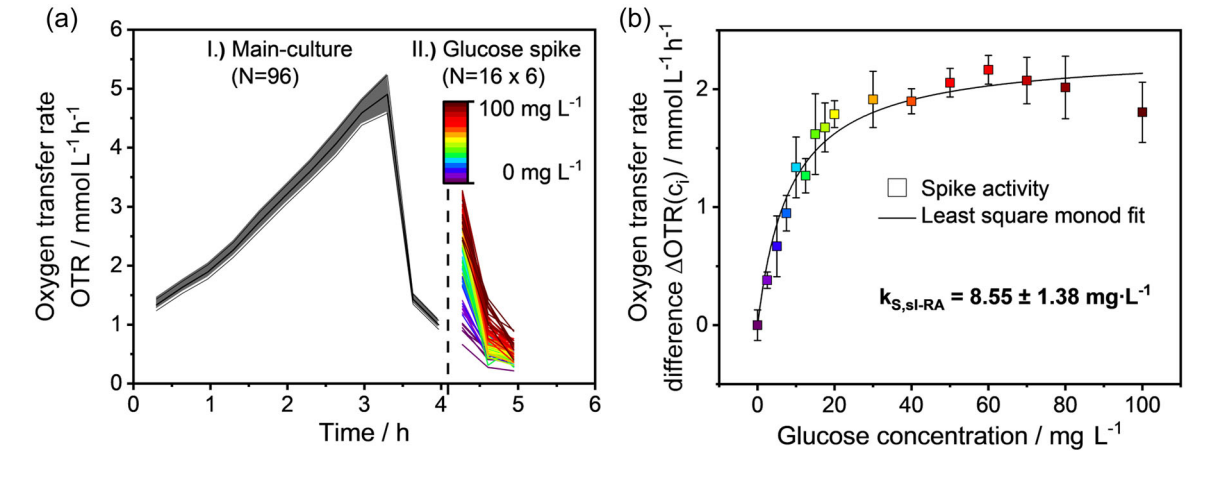


**FIGURE 5** Substrate limited respiratory activity estimation (sl-RA) of the  $k_{\rm S}$  for *Corynebacterium glutamicum* with glucose spiked batch cultivations. (a) Oxygen transfer rates of *C. glutamicum* cultivations (N = 96) spiked with 16 different glucose concentrations (N = 6) after glucose depletion of the main culture. (b) Correlation of the resulting oxygen transfer rate difference after the spike to the respective glucose concentrations with N = 6. Culture conditions: 96-deepwell microtiter plate,  $V_{\rm L} = 1$  mL,  $N_{\rm C} = 0$  mm,  $N_{\rm C} = 0$  mm

1000 10000 100000

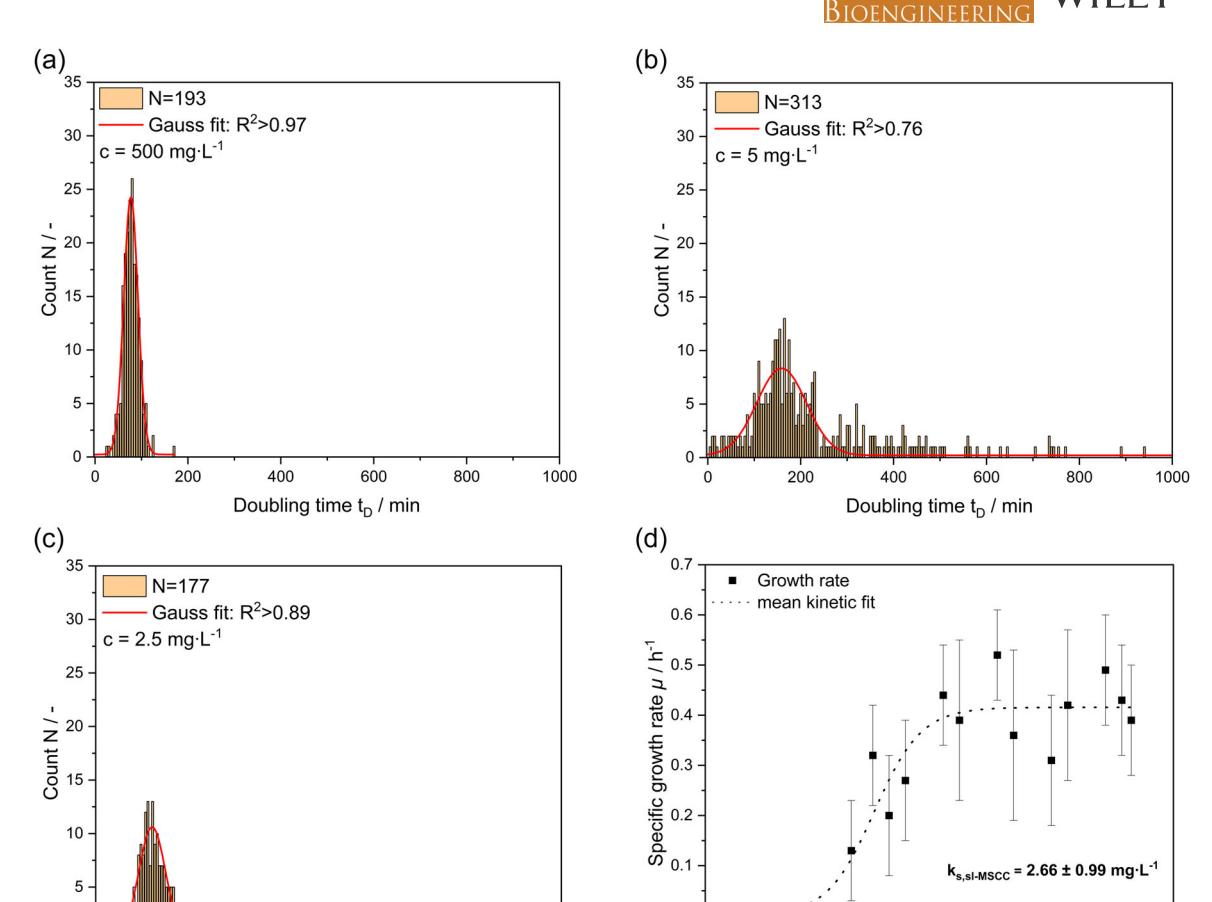


**FIGURE 6** Cumulative distribution of  $t_D$  for at least three biological replicas containing at least 50 single-cell  $t_D$  of *Corynebacterium glutamicum* ATCC 13032 at (a) 500 mg/L, (b) 5 mg/L, (c) 2.5 mg/L glucose in CGXII. (d) Glucose-dependent maximum specific growth rates of individual *C. glutamicum* cells grown in microfluidic perfusion. The black line denotes the fit of the Monod equation to the data set.

0.0

0.01 0.1

limiting growth condition leads to a reduced energy availability for a subpopulation of cells which are struggling to maintain growth. It is reported that under limiting carbon-source conditions, cells have difficulties to maintain optimal growth and cell-to-cell heterogeneity increases (Bettenworth et al., 2019; Lindemann et al., 2019; Martins & Locke, 2015).

400 500 600

Doubling time  $t_{\rm D}$  / min

100 200

Therefore, single-cell  $t_D$  of at least three lineages of a mother cell were analyzed to determine  $\mu$ . Within the observed glucose concentration range from 0 to  $150\,\mathrm{g/L}$ , a Monod-type response was observed (Figure 6d). At concentrations higher than  $500\,\mathrm{mg/L}$ , growth of *C. glutamicum* peaked and remained constant with an observed maximum specific growth rate of  $\mu_{\rm max}=0.41\pm0.02\,h^{-1}$ . At glucose concentrations between 1 mg/L and  $100\,\mathrm{mg/L}$  an increase of doubling time was observed, resulting in reduced cell growth ( $\mu=0.13\pm0.10\,h^{-1}$ ,  $\mu=0.39\pm0.16\,h^{-1}$ ). Glucose concentrations smaller than 1 mg/L resulted in a growth arrest. The regression of the obtained growth data to the Monod equation yielded an average  $k_{\rm S,mean}=2.66\pm0.99\,\mathrm{mg/L}$  with a coefficient of determination of  $R^2=0.87$ .

## 3.3 | Comparison of $k_s$ estimations

Glucose concentration / mg·L-1

The presented methods within this work yielded comparable  $k_s$ values. Moreover, the obtained data are in good agreement with literature values (Table 1). The already published  $k_S$  values for glucose range from 0.52 to 7.68 mg/L, including given standard deviations. Lindner et al. (2011) obtained a value of 2.52 mg/L and Uhde et al. (2013) 2.17-2.70 mg/L by applying liquid scintillation counting. Both values match very well. However, the used protocol of both was highly similar. In these studies, different concentrations of <sup>14</sup>C labeled glucose was supplied to previously washed C. glutamicum cells. After defined time intervals, cell samples are collected and analyzed with a scintillation counter. The data indicate a high reproducibility and a very precise monitoring of glucose uptake rates. Nonetheless, the required equipment and components impede a broad and fast application of this method. In contrast, Graf et al. (2020) utilized enzymatic assays to determine glucose concentrations and deduct glucose consumption rates in batch and chemostat cultivations. Based on a mathematical fit, a  $k_S$  with 4.39 ± 3.20 mg/L

0970290, 2023, 5, Downloaded from https:

Wiley Online Library on [17/08/2023]. See the Term

of use; OA articles are governed by

in batch and  $0.97 \pm 0.45 \, \text{mg/L}$  in chemostat cultivation has been estimated.

While an enzymatic assay for glucose has a detection limit of  $400\,\mu g/L$ , it provides an accurate and fast estimation of residual glucose concentration. However, if the expected affinity toward glucose is higher and consequently below the detection limit, liquid scintillation counting or HPLC are necessary. Interestingly, the authors note different  $k_S$  values for batch and chemostat cultivations but do not elaborate on the reason because the work had a different focus. This differentiation of batch and continuous cultivation for  $k_S$  value estimation is often neglected. However, the  $k_S$  value is subject to the cell state, duration of cultivation as well as environmental conditions and therefore, can vary between batch and chemostat cultivations. Reasons for the deviations could include the washout of slower growing cells due to the set dilution rate or the continuous supply of PCA as a secondary carbon source during chemostat cultivation (Bäumchen et al., 2007).

In addition to the aforementioned established methods, three alternative methods for  $k_S$  estimation are presented in this work. HFB and sI-RA are advantageous with their fast and, in the case of the sI-RA, simple estimation approach. Even though, the estimated  $k_S$  values suggest that sI-RA  $(8.55 \pm 1.38 \text{ mg/L})$  and HFB (<70.7 mg/L with 95%)probability) are not advisable for investigations below concentrations of 10 mg/L. For HFB, the temporal resolution of the BioLector-based biomass observations is limiting, at least for the presented application example with C. glutamicum and glucose as carbon source, resulting in a sharp switch from exponential to stationary phase growth. The increased  $k_s$  value for the sl-RA compared with the sl-MSCC method is partially explained by an inherent overestimation due to the measurement principle. Oxygen partial pressure values are averaged within the required measurement time frame for OTR determination. However, for the  $k_S$  estimation, the initial glucose concentrations are assumed. This effect becomes more prominent with further increased

lengths of the measurement phase (Supporting Information: \$18). Similar to HFB, this overestimation depends on the sharpness of the switch from exponential to stationary phase and, therefore, on the  $k_{\rm S}$ value. In contrast, a k<sub>S</sub> value under defined environmental conditions was obtained by the sl-MSCC approach (2.66 ± 0.99 mg/L). This method is applicable in concentration ranges below 1 mg/L. The image acquisition frequency for determining  $t_D$  plays an essential role. A division event may be documented one frequency interval later than it occurred, leading to increased deviations of the determined  $t_D$ . This aspect is compensated by the number of individual cells tracked and counted. Therefore, the experimental and evaluation throughput of this method must be further increased. For initial estimations or situations where the  $k_S$  value is expected to be rather in the higher mg/L range, HFB and sl-RA can be taken into consideration due to the reduced labor intensity. The sl-MSCC method can yield similar results as lab-scale fermentations in combination with liquid scintillation counting or enzymatic assays. Moreover, sl-MSCC data contains additional information about cellto-cell heterogeneities, which will be discussed in the following section.

#### 3.4 | Potential of sl-MSCC

In contrast to the presented microtiter plate methods, sl-MSCC allows, in addition to  $k_{\rm S}$  determination, insights into cell-to-cell heterogeneity regarding growth and  $t_{\rm D}$  at different cultivation concentrations. For the assurance of a steady state during cultivation, the cumulative distribution of the  $t_{\rm D}$  was plotted as a function of cell generation for each glucose concentration. Here, a constant distribution of the doubling time of approximately 80 min within the first 10 generations was observed for an applied concentration of 500 mg/L glucose (Figure 7a). Similar trends have been obtained for

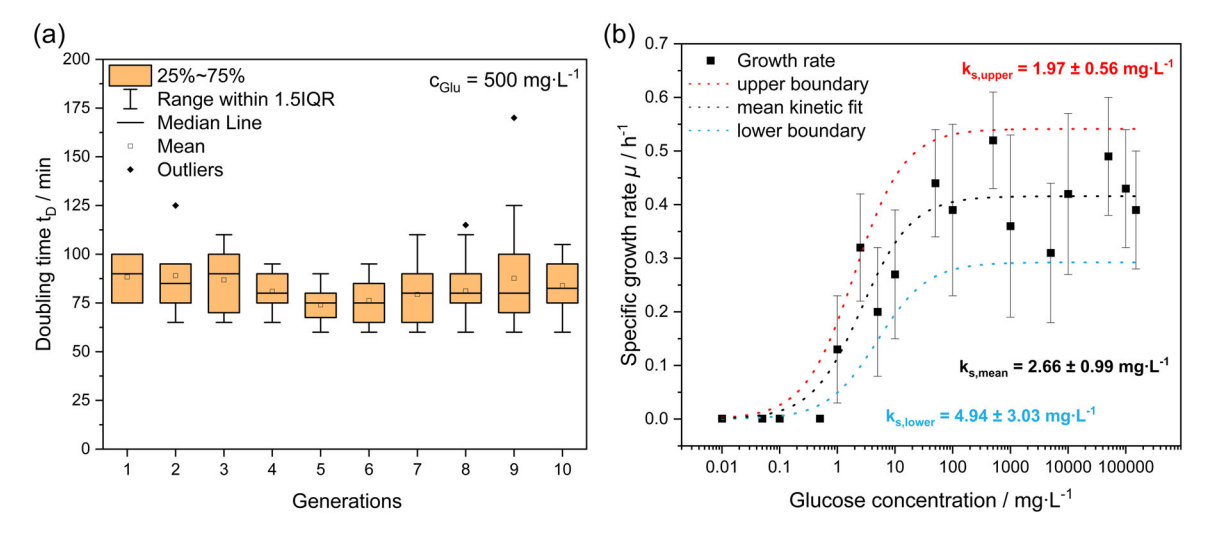


**FIGURE 7** (a) Distribution of single-cell  $t_D$  of individual *Corynebacterium glutamicum* cells as a function of cell generations at a glucose concentration of 500 mg/L. (b) Glucose-dependent maximum specific growth rates of individual *C. glutamicum* cells grown in microfluidic perfusion. The black line denotes the fit of the Monod equation to the data set, while the red and blue lines give the upper and lower boundaries of the mathematical fit, respectively.

Overview of substrate affinities of Corynebacterium glutamicum toward glucose.

Method	Analytics	k <sub>s</sub> (mg/L)	Mode	Reference
<sup>14</sup> C uptake rate	Liquid scintillation counting	2.52	Batch	Lindner et al. (2011)
<sup>14</sup> C uptake rate	Liquid scintillation counting	2.17-2.70	Batch	Uhde et al. (2013)
Consumption rate	Enzymatic assay	4.39 ± 3.20	Batch	Graf et al. (2020)
Consumption rate	Enzymatic assay	0.97 ± 0.45	Chemostat	Graf et al. (2020)
HFB	BioLector	<70.7	Batch	This work
sl-RA	μΤΟΜ	8.55 ± 1.38	Batch	This work
sl-MSCC	Live-cell imaging	2.66 ± 0.99	Perfusion	This work

Abbreviations: HFB, high-frequency biomass; sl-MSCC, substrate-limited microfluidic single-cell cultivation; sl-RA, substrate-limited respiratory activity monitoring; μTOM, micro(μ)-scale Transfer rate Online Measurement.

other glucose concentrations, where steady-state growth lays the foundation for precise determination of  $t_D$  (Supporting Information: S1-S12). The first observation is that a steady state in cell growth and division at constant glucose concentrations of >1 mg/L can be maintained for at least 10 generations (up to the end of the experiment), which corresponds to <2 h/generation. At glucose concentration of ≤1 mg/L steady-state growth cannot be maintained for more than ~4.25 h/generation (Supporting Information: \$13). Here, cell growth declines over the time course of cultivation, resulting even in a stop of growth after eight generations. A possible interpretation can be attributed to the declining storage of carbon sources (Farwick et al., 1995; Koch, 1983; Wolf et al., 2003). The obtained standard deviation, represented by the error bars in Figure 6d represents the cell-to-cell heterogeneity in  $t_D$  of the analyzed cells rather than a statistical error. Thus, 60% of the cells behave within the observed distribution of the average doubling time. This behavior can be used to determine upper and lower boundary values for  $k_S$  because these boundaries can be seen as an approximation of 95% of the cell behavior. Therefore, two additional mathematical fits were made to derive a  $k_s$  from the upper boundary (mean growth rate + standard deviation) and the lower boundary (mean growth rate - standard deviation). The mathematical fit of the estimated data yielded an upper boundary of k<sub>S,upper boundary</sub> =  $1.97 \pm 0.56 \,\text{mg/L}$  and a lower boundary of  $k_{\text{S,lower boundary}} = 4.94 \pm$ 3.03 mg/L with a statistical certainty of the applied regression to the Monod equation of  $R^2 > 0.92$  for the upper boundary and  $R^2 > 0.73$ for the lower boundary (Figure 7b).

In future, further sl-MSCC experiments need to show if and how cells adapt regarding growth and  $t_D$  at different concentrations. The emergence of potential subpopulations has to be analyzed (Arnoldini et al., 2014). These insights help to understand the cellular behavior at limiting conditions and, thus, the dynamics within  $k_S$  values.

The sl-MSCC method needs to be further parallelized, especially to collect statistically relevant numbers of cell division at limiting nutrient concentration ( $c_S < k_S$ ). A critical step is progress in data analysis, which must be automated. In future, by an extension to an oscillation setup, ks values under dynamic environmental conditions

will be accessible, which cannot be measured with any other system (Ho et al., 2022).

#### CONCLUSION

In this work, the recently introduced method of sl-MSCC, which enables the estimation of  $k_S$  by microfluidic perfusion experiments, was revisited and validated for the model organism C. glutamicum ATCC 13032 with glucose as limiting substrate and compared to HFB and sl-RA. Model-based Bayesian inference based on HFB is a rapid and extendible method to estimate the upper limits of  $k_s$ , where the possibility of estimating lower limits is directly dependent on the temporal resolution of the measurements. The sl-RA is an innovative and fast method that provides more precise values than HFB, because of the higher temporal resolution provided through online OTR measurement. However, for estimations of the  $k_s$  under defined environmental conditions, sl-MSCC in combination with livecell imaging seems to be a superior technology because it provides insights into growth behavior at and below the substrate affinity, provides access to cell-lineage information and to single-cell heterogeneity. This enables to model a growth kinetic based on actual observed single-cell growth data without extrapolation. Additionally, sl-MSCC can be used to investigate the influence of cell-to-cell heterogeneity on bulk ks values. The sl-MSCC gives insights into growth deviation and adaptation compared to HFB and sl-RA. In future, sl-MSCC may provide strain-specific  $k_S$  values to tackle the lack of availability. Furthermore, with the extension to an oscillation setup, affinities under fluctuating environmental conditions can be analyzed for the first time in future.

#### **AUTHOR CONTRIBUTIONS**

Conceptualization: Heiko Steinhoff and Alexander Grünberger. Methodology: Heiko Steinhoff, Maurice Finger, Michael Osthege, Simone Schito, Stephan Noack, Jochen Büchs, and Alexander Grünberger. Formal analysis: Heiko Steinhoff, Maurice Finger, Michael Osthege, Stephan Noack, Jochen Büchs, and Alexander Grünberger. Investigation: Heiko

.0970290, 2023, 5, Downloaded from https://onlinelibrary.wiley.com/doi/10.1002/bit.28345 by Forschun

Jülich GmbH Research Center,

Wiley Online Library on [17/08/2023]. See the Terms

for rules of use; OA articles are governed by the applicable Creative Comn

Steinhoff, Maurice Finger, Michael Osthege, Corinna Golze, Stephan Noack, Jochen Büchs, and Alexander Grünberger. *Resources*: Stephan Noack, Jochen Büchs, and Alexander Grünberger. *Writing-original draft preparation*: Heiko Steinhoff, Maurice Finger, and Alexander Grünberger. *Writing-review and editing*: Heiko Steinhoff, Maurice Finger, Michael Osthege, Simone Schito, Stephan Noack, Jochen Büchs, and Alexander Grünberger. *Visualization*: Heiko Steinhoff, Maurice Finger, and Michael Osthege. *Supervision*: Heiko Steinhoff, Maurice Finger, Michael Osthege, Stephan Noack, Jochen Büchs, and Alexander Grünberger. *Project administration*: Heiko Steinhoff and Maurice Finger. *Funding acquisition*: Stephan Noack, Jochen Büchs, and Alexander Grünberger. All authors have read and agreed to the published version of the manuscript.

#### **ACKNOWLEDGMENTS**

Heiko Steinhoff and Alexander Grünberger gratefully acknowledge the support and funding from the Deutsche Forschungsgemeinschaft (priority program SPP2170, project no. 428038451). Maurice Finger and Jochen Büchs gratefully acknowledge support and funding from the Deutsche Forschungsgemeinschaft (priority program SPP2170, project no. 427899901). Michael Osthege, Simone Schito, and Stephan Noack gratefully acknowledge support and funding from the Deutsche Forschungsgemeinschaft (priority program SPP2170, project no. 427904493) and the German Federal Ministry of Education and Research (BMBF, grant no. 031B0463A) as part of the project "Digitalization In Industrial Biotechnology," DigInBio. Open Access funding enabled and organized by Projekt DEAL.

#### CONFLICT OF INTEREST STATEMENT

The authors declare no conflict of interest.

#### DATA AVAILABILITY STATEMENT

The data that support the findings of this study are available from the corresponding author upon reasonable request.

#### **ORCID**

Heiko Steinhoff https://orcid.org/0000-0003-0536-2134

Maurice Finger https://orcid.org/0000-0001-7384-8625

Stephan Noack http://orcid.org/0000-0001-9784-3626

## **REFERENCES**

- Arnoldini, M., Vizcarra, I. A., Peña-Miller, R., Stocker, N., Diard, M., Vogel, V., Beardmore, R. E., Hardt, W. D., & Ackermann, M. (2014). Bistable expression of virulence genes in salmonella leads to the formation of an antibiotic-tolerant subpopulation. *PLoS Biology*, 12(8), e1001928. https://doi.org/10.1371/journal.pbio.1001928
- Bäumchen, C., Knoll, A., Husemann, B., Seletzky, J., Maier, B., Dietrich, C., Amoabediny, G., & Büchs, J. (2007). Effect of elevated dissolved carbon dioxide concentrations on growth of Corynebacterium glutamicum on D-glucose and L-lactate. Journal of Biotechnology, 128(4), 868–874. https://doi.org/10.1016/j.jbiotec.2007.01.001
- Becker, J., Rohles, C. M., & Wittmann, C. (2018). Metabolically engineered Corynebacterium glutamicum for bio-based production of chemicals, fuels, materials, and healthcare products. Metabolic Engineering, 50, 122–141. https://doi.org/10.1016/j.ymben.2018.07.008

- Bettenworth, V., Steinfeld, B., Duin, H., Petersen, K., Streit, W. R., Bischofs, I., & Becker, A. (2019). Phenotypic heterogeneity in bacterial quorum sensing systems. *Journal of Molecular Biology*, 431(23), 4530–4546. https://doi.org/10.1016/j.jmb.2019.04.036
- Burmeister, A., Akhtar, Q., Hollmann, L., Tenhaef, N., Hilgers, F., Hogenkamp, F., Sokolowsky, S., Marienhagen, J., Noack, S., Kohlheyer, D., & Grünberger, A. (2021). (Optochemical) control of synthetic microbial coculture interactions on a microcolony level. ACS Synthetic Biology, 10(6), 1308–1319. https://doi.org/10.1021/acssynbio.0c00382
- Bylund, F., Collet, E., Enfors, S. O., & Larsson, G. (1998). Substrate gradient formation in the large-scale bioreactor lowers cell yield and increases by-product formation. *Bioprocess Engineering*, 18(3), 171–180. https://doi.org/10.1007/s004490050427
- Dinger, R., Lattermann, C., Flitsch, D., Fischer, J. P., Kosfeld, U., & Büchs, J. (2022). Device for respiration activity measurement enables the determination of oxygen transfer rates of microbial cultures in shaken 96-deepwell microtiter plates. *Biotechnology and Bioengineering*, 119(3), 881–894. https://doi.org/10.1002/bit.28022
- Enfors, S. O., Jahic, M., Rozkov, A., Xu, B., Hecker, M., Jürgen, B., Krüger, E., Schweder, T., Hamer, G., O'Beirne, D., Noisommit-Rizzi, N., Reuss, M., Boone, L., Hewitt, C., McFarlane, C., Nienow, A., Kovacs, T., Trägårdh, C., Fuchs, L., Manelius, Å. (2001). Physiological responses to mixing in large scale bioreactors. *Journal of Biotechnology*, 85(2), 175–185. https://doi.org/10.1016/S0168-1656(00)00365-5
- Farwick, M., Siewe, R. M., & Krämer, R. (1995). Glycine betaine uptake after hyperosmotic shift in Corynebacterium glutamicum. Journal of Bacteriology, 177(16), 4690-4695. https://doi.org/10.1128/jb.177. 16.4690-4695.1995
- Ferenci, T. (1999). Growth of bacterial cultures' 50 years on: Towards an uncertainty principle instead of constants in bacterial growth kinetics. Research in Microbiology, 150(7), 431–438. https://doi.org/10.1016/s0923-2508(99)00114-x
- Freudl, R. (2017). Beyond amino acids: Use of the Corynebacterium glutamicum cell factory for the secretion of heterologous proteins. Journal of Biotechnology, 258, 101–109. https://doi.org/10.1016/j.jbiotec.2017.02.023
- Goudar, C. T., & Strevett, K. A. (1998). Estimating growth kinetics of Penicillium chrysogenum through the use of respirometry. Journal of Chemical Technology & Biotechnology, 72(3), 207–212. https://doi. org/10.1002/(SICI)1097-4660(199807)72:3<207::AID-JCTB899>3.
- Graf, M., Haas, T., Teleki, A., Feith, A., Cerff, M., Wiechert, W., Nöh, K., Busche, T., Kalinowski, J., & Takors, R. (2020). Revisiting the growth modulon of *Corynebacterium glutamicum* under glucose limited chemostat conditions. *Frontiers in Bioengineering and Biotechnology*, 8, 584614. https://doi.org/10.3389/fbioe.2020.584614
- Grünberger, A., Probst, C., Heyer, A., Wiechert, W., Frunzke, J., & Kohlheyer, D. (2013). Microfluidic picoliter bioreactor for microbial single-cell analysis: Fabrication, system setup, and operation. *Journal of Visualized Experiments: JoVE*, 82, 50560. https://doi.org/10.3791/50560
- Harrison, D. E. F. (1973). Studies on the affinity of methanol- and methane-utilizing bacteria for their carbon substrates. *Journal of Applied Bacteriology*, 36(2), 301–308. https://doi.org/10.1111/j. 1365-2672.1973.tb04106.x
- Helleckes, L. M., Osthege, M., Wiechert, W., von Lieres, E., & Oldiges, M. (2022). Bayesian calibration, process modeling and uncertainty quantification in biotechnology. *PLoS Computational Biology*, 18(3), e1009223. https://doi.org/10.1371/journal.pcbi.1009223
- Hermann, T. (2003). Industrial production of amino acids by coryneform bacteria. *Journal of Biotechnology*, 104(1–3), 155–172. https://doi.org/10.1016/S0168-1656(03)00149-4
- Ho, P., Täuber, S., Stute, B., Grünberger, A., & von Lieres, E. (2022). Microfluidic reproduction of dynamic bioreactor environment based

- on computational lifelines. Frontiers in Chemical Engineering, 4,
- Ihling, N., Munkler, L. P., Berg, C., Reichenbächer, B., Wirth, J., Lang, D., Wagner, R., & Büchs, J. (2021). Time-resolved monitoring of the oxygen transfer rate of Chinese hamster ovary cells provides insights into culture behavior in shake flasks. Frontiers in Bioengineering and Biotechnology, 9, 725498. https://doi.org/10.3389/fbioe.2021.725498

826485. https://doi.org/10.3389/fceng.2022.826485

- Junker, B. H. (2004). Scale-up methodologies for Escherichia coli and yeast fermentation processes. *Journal of Bioscience and Bioengineering*, 97(6), 347–364. https://doi.org/10.1016/S1389-1723(04)70218-2
- Kell, D. B., & Sonnleitner, B. (1995). GMP-good modelling practice: An essential component of good manufacturing practice. *Trends in Biotechnology*, 13(11), 481–492. https://doi.org/10.1016/S0167-7799(00)89006-X
- Koch, A. L. (1983). The surface stress theory of microbial morphogenesis. Advances in Microbial Physiology, 24, 301–366. https://doi.org/10. 1016/S0065-2911(08)60388-4
- Kovárová-Kovar, K., & Egli, T. (1998). Growth kinetics of suspended microbial cells: From single-substrate-controlled growth to mixedsubstrate kinetics. Microbiology and Molecular Biology Reviews, 62(3), 646–666. https://doi.org/10.1128/MMBR.62.3.646-666.1998
- Legan, J. D., & Owens, J. D. (1987). Determination of growth parameters of methylamine-using bacteria. *Microbiology*, 133(4), 1075–1080. https://doi.org/10.1099/00221287-133-4-1075
- Li, Y., Jin, M., O'Laughlin, R., Bittihn, P., Tsimring, L. S., Pillus, L., Hasty, J., & Hao, N. (2017). Multigenerational silencing dynamics control cell aging. Proceedings of the National Academy of Sciences, 114(42), 11253–11258. https://doi.org/10.1073/pnas.1703379114
- Liebl, W., Klamer, R., & Schleifer, K. H. (1989). Requirement of chelating compounds for the growth of *Corynebacterium glutamicum* in synthetic media. *Applied Microbiology and Biotechnology*, 32(2), 205–210. https://doi.org/10.1007/BF00165889
- Lindemann, D., Westerwalbesloh, C., Kohlheyer, D., Grünberger, A., & von Lieres, E. (2019). Microbial single-cell growth response at defined carbon limiting conditions. *RSC Advances*, *9*(25), 14040–14050. https://doi.org/10.1039/c9ra02454a
- Lindner, S. N., Seibold, G. M., Henrich, A., Krämer, R., & Wendisch, V. F. (2011). Phosphotransferase system-independent glucose utilization in *Corynebacterium glutamicum* by inositol permeases and glucokinases. *Applied and Environmental Microbiology*, 77(11), 3571–3581. https://doi.org/10.1128/AEM.02713-10
- Mandenius, C.-F. (Ed.). (2016). Bioreactors: Design, operation and novel applications (1st ed.). Wiley-VCH. http://nbn-resolving.org/urn: nbn:de:bsz:31-epflicht-1081908
- Martin, O., Hartikainen, A., Abril-Pla, C. O., Kumar, R., Gautam, P., Arroyuelo, A., Naeem, R., Banerjea, R. A., Pasricha, N., Gruevski, P., Sanjay, R., Rochford, A., Phan, D., Mahweshwari, U., Kazantsev, V., Arunava, Andorra, A., & Lozada, R. P. (2021). ArviZ. Zenodo.
- Martins, B. M., & Locke, J. C. (2015). Microbial individuality: How singlecell heterogeneity enables population level strategies. Current Opinion in Microbiology, 24, 104–112. https://doi.org/10.1016/j. mib.2015.01.003
- Monod, J. (1949). The growth of bacterial cultures. Annual Review of Microbiology, 3(1), 371–394. https://doi.org/10.1146/annurev.mi. 03.100149.002103
- Mühlmann, M. J., Forsten, E., Noack, S., & Büchs, J. (2018). Prediction of recombinant protein production by *Escherichia coli* derived online from indicators of metabolic burden. *Biotechnology Progress*, 34(6), 1543–1552. https://doi.org/10.1002/btpr.2704
- Oliveira, C. S., Ordaz, A., Alba, J., Alves, M., Ferreira, E. C., & Thalasso, F. (2009). Determination of kinetic and stoichiometric parameters of *Pseudomonas putida* F1 by chemostat and in situ pulse respirometry. Chemical Product and Process Modeling, 4(2). https://doi.org/10.2202/1934-2659.1304

- Ordaz, A., Oliveira, C. S., Aguilar, R., Carrión, M., Ferreira, E. C., Alves, M., & Thalasso, F. (2008). Kinetic and stoichiometric parameters estimation in a nitrifying bubble column through "in-situ" pulse respirometry. *Biotechnology and Bioengineering*, 100(1), 94–102. https://doi.org/10.1002/bit.21723
- Osthege, M., & Helleckes, L. M. (2022a). JuBiotech/calibr8: v6.4.0. Zenodo.
- Osthege, M., & Helleckes, L. M. (2022b). JuBiotech/murefi: v5.1.0. Zenodo.
- Osthege, M., & Schito, S. (2022). Supplement to Experimental  $k_S$  estimation: A comparison of methods for *Corynebacterium glutamicum* from lab to microfluidic scale. Zenodo.
- Osthege, M., Tenhaef, N., Helleckes, L. M., & Müller, C. (2022). JuBiotech/bletl: v1.1.0. Zenodo.
- Osthege, M., Tenhaef, N., Zyla, R., Müller, C., Hemmerich, J., Wiechert, W., Noack, S., & Oldiges, M. (2022). bletl A Python package for integrating BioLector microcultivation devices in the Design-Build-Test-Learn cycle. *Engineering in Life Sciences*, 22(3-4), 242–259. https://doi.org/10.1002/elsc.202100108
- Phoenix, D. (1997). Introductory mathematics for the life sciences. Modules in life sciences. CRC Press.
- Schindelin, J., Arganda-Carreras, I., Frise, E., Kaynig, V., Longair, M., Pietzsch, T., Preibisch, S., Rueden, C., Saalfeld, S., Schmid, B., Tinevez, J. Y., White, D. J., Hartenstein, V., Eliceiri, K., Tomancak, P., & Cardona, A. (2012). Fiji: An open-source platform for biological-image analysis. *Nature Methods*, 9(7), 676–682. https://doi.org/10.1038/nmeth.2019
- Schmideder, A., Severin, T. S., Cremer, J. H., & Weuster-Botz, D. (2015). A novel milliliter-scale chemostat system for parallel cultivation of microorganisms in stirred-tank bioreactors. *Journal of Biotechnology*, 210, 19–24. https://doi.org/10.1016/j.jbiotec.2015.06.402
- Senn, H., Lendenmann, U., Snozzi, M., Hamer, G., & Egli, T. (1994). The growth of Escherichia coli in glucose-limited chemostat cultures: A re-examination of the kinetics. Biochimica Et Biophysica Acta (BBA)-General Subjects, 1201(3), 424–436. https://doi.org/10.1016/0304-4165(94)90072-8
- Stöckmann, C., Maier, U., Anderlei, T., Knocke, C., Gellissen, G., & Büchs, J. (2003). The oxygen transfer rate as key parameter for the characterization of *Hansenula polymorpha* screening cultures. *Journal of Industrial Microbiology* & *Biotechnology*, 30(10), 613–622. https://doi.org/10.1007/s10295-003-0090-9
- Takors, R. (2012). Scale-up of microbial processes: Impacts, tools and open questions. *Journal of Biotechnology*, 160(1-2), 3-9. https://doi. org/10.1016/j.jbiotec.2011.12.010
- Täuber, S., Golze, C., Ho, P., von Lieres, E., & Grünberger, A. (2020). dMSCC: a microfluidic platform for microbial single-cell cultivation of *Corynebacterium glutamicum* under dynamic environmental medium conditions. *Lab on a Chip*, 20(23), 4442–4455. https://doi.org/10.1101/2020.07.10.188938
- ter Braak, C. J. F., & Vrugt, J. A. (2008). Differential evolution Markov chain with snooker updater and fewer chains. *Statistics and Computing*, 18(4), 435–446. https://doi.org/10.1007/s11222-008-9104-9
- Toepke, M. W., & Beebe, D. J. (2006). PDMS absorption of small molecules and consequences in microfluidic applications. *Lab on a Chip*, 6(12), 1484–1486. https://doi.org/10.1039/b612140c
- Uhde, A., Youn, J. W., Maeda, T., Clermont, L., Matano, C., Krämer, R., Wendisch, V. F., Seibold, G. M., & Marin, K. (2013). Glucosamine as carbon source for amino acid-producing *Corynebacterium glutamicum*. Applied Microbiology and Biotechnology, 97(4), 1679–1687. https://doi.org/10.1007/s00253-012-4313-8
- Unthan, S., Grünberger, A., van Ooyen, J., Gätgens, J., Heinrich, J., Paczia, N., Wiechert, W., Kohlheyer, D., & Noack, S. (2014). Beyond growth rate 0.6: What drives Corynebacterium glutamicum to higher growth rates in defined medium. Biotechnology and Bioengineering, 111(2), 359-371. https://doi.org/10.1002/bit.25103

- Vertès, A. A., Inui,M., & Yukawa, H. (2012). Postgenomic approaches to using corynebacteria as biocatalysts. *Annual Review of Microbiology*, 66, 521–550. https://doi.org/10.1146/annurevmicro-010312-105506
- von der Osten, C. H., Gioannetti, C., & Sinskey, A. J. (1989). Design of a defined medium for growth of *Corynebacterium glutamicum* in which citrate facilitates iron uptake. *Biotechnology Letters*, 11(1), 11–16. https://doi.org/10.1007/BF01026778
- Wang, P., Robert, L., Pelletier, J., Dang, W. L., Taddei, F., Wright, A., & Jun, S. (2010). Robust growth of Escherichia coli. Current Biology, 20(12), 1099–1103. https://doi.org/10.1016/j.cub.2010.04.045
- Wechselberger, P., Sagmeister, P., & Herwig, C. (2013). Real-time estimation of biomass and specific growth rate in physiologically variable recombinant fed-batch processes. *Bioprocess and Biosystems Engineering*, 36(9), 1205–1218. https://doi.org/10.1007/s00449-012-0848-4
- Wendisch, V. F., Bott, M., & Eikmanns, B. J. (2006). Metabolic engineering of Escherichia coli and Corynebacterium glutamicum for biotechnological production of organic acids and amino acids. Current Opinion in Microbiology, 9(3), 268–274. https://doi.org/10.1016/j. mib.2006.03.001
- Wendisch, V. F., Jorge, J., Pérez-García, F., & Sgobba, E. (2016). Updates on industrial production of amino acids using *Corynebacterium glutamicum*. World Journal of Microbiology & Biotechnology, 32(6), 105. https://doi.org/10.1007/s11274-016-2060-1

- Wiecki, T., Salvatier, J., Patil, A., Kochurov, M., Engels, B., Lao, J., Colin Martin, O., Ricardo, V., Willard, B. T., & Osthege, M. (2022). pymc-devs/pymc: v4.0.0b2. Zenodo.
- Wolf, A., Krämer, R., & Morbach, S. (2003). Three pathways for trehalose metabolism in *Corynebacterium glutamicum* ATCC13032 and their significance in response to osmotic stress. *Molecular Microbiology*, 49(4), 1119–1134. https://doi.org/10.1046/j.1365-2958.2003. 03625.x

#### SUPPORTING INFORMATION

Additional supporting information can be found online in the Supporting Information section at the end of this article.

How to cite this article: Steinhoff, H., Finger, M., Osthege, M., Golze, C., Schito, S., Noack, S., Büchs, J., & Grünberger, A. (2023). Experimental  $k_{\rm S}$  estimation: A comparison of methods for *Corynebacterium glutamicum* from lab to microfluidic scale. *Biotechnology and Bioengineering*, 120, 1288–1302.

https://doi.org/10.1002/bit.28345